This is the Pre-Published Version.

This is the peer reviewed version of the following article: An, S, Zhu, X, Shen, M, et al. Mismatch in elevational shifts between satellite observed vegetation greenness and temperature isolines during 2000–2016 on the Tibetan Plateau. Glob Change Biol. 2018; 24: 5411– 5425, which has been published in final form at https://doi.org/10.1111/gcb.14432. This article may be used for non-commercial purposes in accordance with Wiley Terms and Conditions for Use of Self-Archived Versions. This article may not be enhanced, enriched or otherwise transformed into a derivative work, without express permission from Wiley or by statutory rights under applicable legislation. Copyright notices must not be removed, obscured or modified. The article must be linked to Wiley's version of record on Wiley Online Library and any embedding, framing or otherwise making available the article or pages thereof by third parties from platforms, services and websites other than Wiley Online Library must be prohibited.

Accepted Article

DR. MIAOGEN SHEN (Orcid ID : 0000-0001-5742-8807)

Article type : Primary Research Articles

Mismatch in elevational shifts between satellite observed vegetation greenness and temperature isolines during 2000-2016 on the Tibetan Plateau

Keywords

Climate warming, elevational shift, grassland, Tibetan Plateau, vegetation greenness, velocity

Running title

Mismatch between greenness and temperature

Shuai AN[1], Xiaolin ZHU[3], Miaogen SHEN[2*], Yafeng WANG[2*], Ruyin CAO[4], Xuehong CHEN[5], Wei YANG[6], Jin CHEN[5] , Yanhong TANG[7]

[1] College of Applied Arts and Science, Beijing Union University, 197 Beitucheng West Rd, Haidian District, Beijing 100191, China. anshuai@buu.edu.cn

[2] Key Laboratory of Alpine Ecology and Biodiversity, CAS Center for Excellence in Tibetan Plateau Earth Sciences, Institute of Tibetan Plateau Research, Chinese Academy of Sciences, 16 Lincui Rd, Chaoyang District, Beijing 100101, China.

This article has been accepted for publication and undergone full peer review but has not been through the copyediting, typesetting, pagination and proofreading process, which may lead to differences between this version and the Version of Record. Please cite this article as doi: 10.1111/gcb.14432
This article is protected by copyright. All rights reserved.

[3] Department of Land Surveying and Geo-Informatics, The Hong Kong Polytechnic University, 181 Chatham Road South, Hung Hom, Kowloon, Hong Kong. xiaolin.zhu@polyu.edu.hk

[4] School of Resources and Environment, University of Electronic Science and Technology of China, 2006 Xiyuan Avenue, West Hi-tech Zone, Chengdu, Sichuan 611731, China. cao.ruyin@uestc.edu.cn

[5] State Key Laboratory of Earth Surface Processes and Resource Ecology, College of Remote Sensing Science and Engineering, Faculty of Geographical Science, Beijing Normal University, Beijing 100875, China. chenxuehong@bnu.edu.cn, chenjin@bnu.edu.cn

[6] Center for Environmental Remote Sensing, Chiba University, 1-33, Yayoicho Inageku Chibashi, Chibaken, 263-8522, Japan. yangwei@chiba-u.jp

[7] Department of Ecology, College of Urban and Environmental Sciences, and Key Laboratory for Earth Surface Processes of the Ministry of Education, Peking University. Beijing 100871, China. tangyh@pku.edu.cn

*Corresponding authors: Miaogen SHEN, shen.miaogen@gmail.com; Yafeng WANG, yfwang@rcees.ac.cn

Abstract

Climate warming on the Tibetan Plateau tends to induce an uphill shift of temperature isolines. Observations and process-based models have both shown that climate warming has resulted in an increase in vegetation greenness on the Tibetan Plateau in recent decades. However, it is unclear whether the uphill shift of temperature isolines has caused greenness isolines to shift upward and whether the two shifts match each other. Our analysis of satellite observed vegetation greenness during the growing season (May–Sep) and gridded climate data for 2000–2016 documented a substantial mismatch between the elevational shifts of greenness and temperature isolines. This mismatch is probably associated with a lagging response of greenness to temperature change and with the elevational gradient of greenness. The lagging response of greenness may be associated with water limitation, resources availability, and acclimation. This lag may weaken carbon sequestration by Tibetan ecosystems, given that greenness is closely related to primary carbon uptake and ecosystem respiration increases exponentially with temperature. We also found that differences in terrain slope angle accounted for large spatial variations in the elevational gradient of greenness and thus the velocity of elevational shifts of greenness isolines and the sensitivity of elevational shifts of greenness isolines to temperature, highlighting the role of terrain effects on the elevational shifts of greenness isolines. The mismatches and the terrain effect found in this study suggest that there is potentially large micro-topographical difference in response and acclimation/adaptation of greenness to temperature changes in plants. More widespread in situ measurements and fine-resolution remote sensing observations and fine gridded climate data are required to attribute the mismatch to specific environmental drivers and ecological processes such as vertical changes in community structure, plant physiology, and distribution of species.

Introduction

Observations from around the world have shown that the rate of temperature increase during the past few decades was greater at high elevations than at low elevations (Mountain-Research-Initiative-EDW-Working-Group, 2015). This pattern of elevation-dependent warming is expected to modify biodiversity, vegetation greenness-a surrogate of aboveground green biomass or leaf area index, carbon and water cycles, energy flows, and other functions in mountain ecosystems (Alexander *et al.*, 2018, Crimmins *et al.*, 2011, Gottfried *et al.*, 2012, Shen *et al.*, 2014). Although many studies have focused on ecosystem changes, such as shifts in species ranges and changes in plant community compositions (Bertrand *et al.*, 2011, Crimmins *et al.*, 2011, Klanderud & Birks, 2003, Lenoir *et al.*, 2008, Saikkonen *et al.*, 2012), few studies have addressed the elevation-dependent relationships between climate warming and greenness which is a proxy for vegetation productivity in mountain areas (Tao *et al.*, 2015). Given that temperature is a major determinant of greenness in alpine regions (Körner, 2003), climate warming should have substantially affected the geographical pattern of greenness. However, relevant data are generally lacking.

The Tibetan Plateau is well suited to investigations of this topic: it is large, with an area of about 2.5 × 10^6 km^2, and it has vegetation widely distributed up to about 6000 m above sea level, well below its highest elevation of 8843 m. Moreover, changes in greenness on the Tibetan Plateau could significantly modify the biophysical properties of the land surface (Shen *et al.*, 2015b), which could in turn affect the movement of air masses over and around the Tibetan Plateau and thus have far-reaching impacts on regional and continental climate (Wu & Liu, 2016, Wu *et al.*, 2012, Zhang *et al.*, 2011). Changes in greenness also play an important role in the area's carbon balance, which is sensitive to climate change (Piao *et al.*, 2012).

The Tibetan Plateau has experienced intensive climate warming in recent decades at a rate of about 0.4 °C per decade (Bibi *et al.*, 2018, Dong *et al.*, 2012, Duan & Xiao, 2015, Mountain-Research-Initiative-EDW-Working-Group, 2015, Xu *et al.*, 2017). Moreover, unlike the global warming "hiatus" since 1998 elsewhere, the temperature continued to increase on the Tibetan Plateau (Duan & Xiao, 2015, Xu *et al.*, 2017). Satellite observations and process-based ecosystem model simulations have both explained increases in greenness as a result of this warming (Piao *et al.*, 2012, Shen *et al.*, 2015b, Wang *et al.*, 2012). However, although temperature has been shown to increase faster at higher elevations on the Tibetan Plateau (Mountain-Research-Initiative-EDW-Working-Group, 2015), it is yet not clear whether greenness has likewise increased faster at higher elevations. Moreover, it is unclear whether the rate of increase with respect to elevation is the same for climate warming and greenness. It is well understood that climate warming results in uphill movement of temperature isolines on the Tibetan Plateau. Given that greenness declines with elevation, we should expect greenness to respond to climate change with an uphill shift of greenness isolines on the Tibetan Plateau. Whether the upward progress of warming matches the upward increase in greenness is subject to how greenness responds to temperature; however, some studies have shown that the response of greenness to temperature on the Tibetan Plateau is nonlinear and spatially diverse (Cong *et al.*, 2017, Dorji *et al.*, 2013, Shen *et al.*, 2015a, Wang *et al.*, 2015a). In addition, field observations across the plateau show that warming-induced upward shifts of treelines were slowed by species interactions (Liang *et al.*, 2016, Wang *et al.*, 2016). Those observations (Liang *et al.*, 2016, Wang *et al.*, 2016) imply that the elevational shifts of greenness isolines may be affected by biotic factors, although there are differences between greenness isolines and treelines. Those studies suggest that elevational shifts of greenness isolines may have a complex relationship with shifts of temperature isolines on the Tibetan Plateau.

Vegetation indices derived from time series of satellite images have been widely used to quantify vegetation greenness and monitor vegetation dynamics. The normalized difference vegetation index (NDVI) is based on the reflectance in the red and near infrared bands, which are closely related to photosynthetic pigments and mesophyll (Tucker *et al.*, 1986). Satellite-derived NDVI has been shown to be directly related to the aboveground green biomass of the canopy and vegetation greenness (Huete *et al.*, 2002, Myneni *et al.*, 1997, Shen *et al.*, 2008), and it has been widely used to indicate changes in large-scale vegetation dynamics and greenness (Edwards & Treitz, 2017, Guay *et al.*, 2014, Xu *et al.*, 2013). Thus, NDVI time series offer an opportunity to investigate the consistency between changes in temperature and greenness on the Tibetan Plateau, where no in situ observations at large scales are available.

In this paper, we first report the elevational pattern of multiyear averages of temperature and vegetation greenness on the Tibetan Plateau using the growing season NDVI ($NDVI_{GS}$), derived from Moderate Resolution Imaging Spectroradiometer (MODIS) imagery. We then address the question of whether or not the uphill movement of temperature isolines matches that of $\mathrm{NDVI}_{\mathrm{GS}}$ isolines during 2000–2016, a period of rapid warming. Lastly, we examine the spatial variations in the rate of elevational movement of $\mathrm{NDVI}_{\mathrm{GS}}$ isolines and explore possible explanations for those variations.

Materials and methods

Datasets

The NDVI data used in this study were extracted from the MOD13Q1 Version 6 product, which was downloaded from https://reverb.echo.nasa.gov during October 2017. The spatial resolution of the data grid is about 250 m. The main approach used to produce this product was the Constrained View angle–Maximum Value Composite (CV-MVC), which generates the best quality NDVI for every 16-day period (resulting in 23 NDVI values per year) using the two 8-day composite surface reflectance granules (MOD09A1) (Didan *et al.*, 2015). This surface reflectance product employs a minimum-blue-band-reflectance approach to minimize contaminations by clouds, aerosols, and other factors (Didan *et al.*, 2015).

The gridded climate data, including daily air temperature and precipitation, were extracted from a dataset produced by the Data Assimilation and Modeling Center for Tibetan Multi-spheres, Institute of Tibetan Plateau Research, Chinese Academy of Sciences (Chen *et al.*, 2011, He, 2010). The climate variables were produced for every 3 hours at a spatial resolution of 0.1° × 0.1°. Air temperature at 2 m above the ground surface was produced by assimilating meteorological records at stations provided by the China Meteorological Administration (CMA) and the Princeton meteorological forcing data (Sheffield *et al.*, 2006). The precipitation data were produced by assimilating the precipitation observations at the operational stations of CMA, the precipitation data provided by the Asian Precipitation - Highly Resolution Observational Data Integration Toward Evaluation of the Water Resources (APHRODITE) (Yatagai *et al.*, 2009) and the Tropical Rainfall Measuring Mission (TRMM) 3B42 (Huffman *et al.*, 2007).

The elevation data were provided by the Advanced Spaceborne Thermal Emission and Reflection Radiometer Global Digital Elevation Model version 2, at a spatial resolution of 30 m, downloaded from http://earthexplorer.usgs.gov/. More information can be found in http://www.jspacesystems.or.jp/ersdac/GDEM/E/1.html. Vegetation types across the Tibetan Plateau were extracted from the 1:1,000,000 Vegetation Atlas of China (Editorial Board of Vegetation Map of China). The vegetation types used in this study included alpine meadow, alpine steppe, alpine cushion vegetation, alpine shrubland, and forest. A map of the distribution of those vegetation types can be found in (Geng *et al.*, 2012).

Analyses

We focused on areas with elevations higher than 3000 m that also had vegetation coverage. Grid cells in the NDVI product (referred to as pixels hereafter) were the basis of our analysis. A pixel with vegetation coverage was determined as follows. First, pixels with multiyear

(2000–2016) average NDVI higher than 0.4 were classified as moderate or dense vegetation coverage. Evergreen vegetation in the southeastern Tibetan Plateau (Geng *et al.*, 2012) belonged to this category. Second, pixels were excluded from further analysis if the lowest annual mean NDVI value over the period 2000–2016 was less than 0.1. Third, pixels with annual mean NDVI between 0.1 and 0.4 were considered to have deciduous vegetation. For those pixels we calculated an average annual NDVI profile (consisting of 23 values), then imposed two criteria to determine if a pixel represented vegetation coverage: 1) the peak maximum NDVI value occurred in summer (June–August) and 2) the summer peak NDVI was at least 1.2 times the average NDVI for January through March. By this means, we excluded pixels with no vegetation coverage, accounting for 55.2% of the total pixels, mainly distributed in the northern and western regions and lakes and glaciers of the plateau. The climate data and vegetation type data then were resampled to the resolution of NDVI data, using the bilinear interpolation method.

Regional level analysis

The regional level analysis focused on 100-m elevation bins for the study area and used growing season NDVI ($NDVI_{GS}$) and growing season temperature (T_{GS}), defined as the mean of the five monthly maximum NDVI values for May to September and the mean daily temperature from May to September, respectively. Here monthly maximum NDVI was used to further eliminate clouds and snow effect on NDVI. Only bins with at least 1000 data points were included in the analysis, and the elevation ranged from 2950–3050 m (the 3000 m bin) to 5650–5750 m (the 5700 m bin). We first calculated the mean of the set of annual $\mathrm{NDVI_{GS}}$ and $\mathrm{T_{GS}}$ values for pixels in each elevation bin. We then calculated the velocity of the vertical movement of $\mathrm{NDVI_{GS}}$ isolines ($\mathrm{V\_NDVI_{GS}}$) at a given elevation bin:

$$\mathrm{V\_NDVI_{GS}}(h) = \frac{\mathrm{T\_NDVI_{GS}}(h)}{\mathrm{A\_NDVI_{GS}}(h)}, \tag{1}$$

where $\mathrm{T\_NDVI_{GS}}(h)$ is the temporal trend of $\mathrm{NDVI_{GS}}$ and $\mathrm{A\_NDVI_{GS}}(h)$ is the elevational gradient of $\mathrm{NDVI_{GS}}$ at elevation bin h. $\mathrm{V\_NDVI_{GS}}$ is measured in meters per year, where positive values indicate upward movement while the negative values are downhill movement (Table 1). $\mathrm{T\_NDVI_{GS}}(h)$ is defined as the slope of the linear regression between $\mathrm{NDVI_{GS}}$ and years, and $\mathrm{A\_NDVI_{GS}}(h)$ is defined from the two neighboring bins as

$$\mathrm{A\_NDVI_{GS}}(h) = \frac{\mathrm{NDVI_{GS}}[(h-100){:}\,h] - \mathrm{NDVI_{GS}}[h{:}(h+100)]}{\mathrm{E}[(h-100){:}\,h] - \mathrm{E}[h{:}(h+100)]}, \tag{2}$$

where E[(h - 100) : h] is the mean of the elevation of all pixels in the interval from h-100 to h, and similar do $\mathrm{E}[h : (h + 100)]$, $\mathrm{NDVI_{GS}}[(h - 100) : h]$, and $\mathrm{NDVI_{GS}}[h : (h + 100)]$. The velocity of vertical movements of $\mathrm{T_{GS}}$ isolines was determined in a similar manner.

We further investigated the sensitivity of movements of $\mathrm{NDVI_{GS}}$ isolines to temperature, $\mathrm{S\_NDVI_{GS}}$, at each elevation bin, defined as

$$\mathrm{S\_NDVI_{GS}}(h) = \frac{\mathrm{L\_NDVI_{GS}\_T}(h)}{\mathrm{A\_NDVI_{GS}}(h)}, \tag{3}$$

where $\mathrm{L\_NDVI_{GS}\_T}(h)$, the change rate of $\mathrm{NDVI_{GS}}$ with respect to $\mathrm{T_{GS}}$, is the coefficient of $\mathrm{T_{GS}}$ in the multiple linear regression model $\mathrm{NDVI_{GS}}(h) \approx \mathrm{T_{GS}}(h) + \mathrm{P}(h)$, in which $\mathrm{P}(h)$ is cumulative precipitation in the growing season, which is included in the regression because precipitation may affect greenness. S_NDVI$_{GS}$(h) is expressed as the change in greenness isolines in meters when the temperature increases by 1°C, positive values signifying upward movement (Table 1).

Pixel level analysis

In the pixel level analysis, the movement velocity of NDVI$_{GS}$ isolines is determined from Eq. (1), but using individual pixels instead of bin averages. The temporal trend of NDVI$_{GS}$ was again determined as the slope in the linear regression between NDVI$_{GS}$ and years. The elevational gradient of NDVI$_{GS}$ for a given pixel was defined as follows. A given pixel and its eight neighbors defined a 3 × 3 pixel window with that pixel in the center. Sets of three pixels defined four directions through the central pixel (Fig. 1): vertical (azimuth 0°), horizontal (90°), and two orthogonal diagonals (45° and 135°). Slopes were determined only for directions with monotonically increasing or decreasing elevation. For each of those directions, we calculated the slope angle for the central pixel using the elevations of the two pixels on opposite sides of it. We determined the elevational gradient of NDVI$_{GS}$ along those directions, wherever NDVI$_{GS}$ increased or decreased monotonically, as the ratio of NDVI$_{GS}$ difference to elevation difference between the two pixels neighboring the central pixel. Here only pixels with slope angle greater than 2.5° were considered, and the direction with the steepest slope was selected. From that result, it was simple to determine the aspect for the central pixel as the slope angle along one of the eight azimuths from 45° to 360°. The pixels with NDVI$_{GS}$ increasing or decreasing monotonically along slope accounted for about 96.5%

of the total vegetated pixels with slope greater than 2.5°. For a given pixel, we determined the sensitivity of movements of $NDVI_{GS}$ isolines to temperature as the ratio defined by the sensitivity of $NDVI_{GS}$ to T_{GS} divided by the elevational gradient of $NDVI_{GS}$, and the first term of this ratio was determined by a regression similar to that in the regional analysis. Positive values of velocity and sensitivity signify upward shifts (Table 1).

Results

Elevation dependence of mean growing season temperature and NDVI

The mean value of T_{GS} for the period 2000–2016 decreased linearly with elevation, from about 11.5 °C at 3000 m to about 3.1 °C at 5700 m (Fig. 2a), and the mean $NDVI_{GS}$ for this period also generally decreased with elevation (Fig. 2b). In detail, the mean $NDVI_{GS}$ increased from about 0.55 in the 3000–3200 m bins to about 0.59 at 3500 m, gradually decreased to about 0.53 at 4200 m, sharply decreased to about 0.30 at 4900 m, then gradually decreased to about 0.22 at 5700 m. In correspondence with T_{GS}, the gradient of T_{GS} with elevation increased between the 3000 m and 4600 m bins and decreased with some fluctuations at higher elevations (Fig. 3a). The gradient was about –5.6 °C/km at 3000–3300 m, about –1 °C/km at 4600–4700 m, and about –3.5 °C/km at 5500–5700 m. The elevational gradient of $NDVI_{GS}$ was about 0 for 3000–3300 m, about 0.25/km at 3400 m, about –0.44/km at 4500 m, about –0.09/km around 5100 m, and about –0.07/km between 5100 and 5700 m (Fig. 3b).

The rate of increase in T_{GS} from 2000 to 2016 rose with elevation from about 0.007 °C/year at 3000 m to about 0.057 °C/year at 4500 m, slowed above that to about 0.046 °C/year at 5000, then rapidly fell above 5300 m, reaching –0.017 °C/year at 5700 m (Fig. 3c). In contrast, the temporal trends of $NDVI_{GS}$ showed a general decrease with elevation, with exceptions in the bins around 3300, 4300, and 5600 m (Fig. 3d). The trend was strongly positive at the lowest elevations, fell to zero by 4800 m, and was weakly negative at all higher elevations except in the top bin, 5700 m.

Elevation dependence of velocity of T_{GS} and $NDVI_{GS}$ isoline movement

Between 2000 and 2016, the T_{GS} isolines moved from lower to higher elevations, except in the two highest bins at 5600 m and 5700 m (Fig. 3e). The velocity of this elevation change increased steadily with increasing elevation, from about 2m/year at 3000 m to about 16 m/year at 5100 m, interrupted by an extreme peak centered at 4600 m that reached about 85 m/year. It then increased to about 33 m/year at 5200 and 5300 m and steeply decreased to about –6 m/year at 5700 m. In contrast, the vertical movement of $NDVI_{GS}$ isolines was generally much smaller (Fig. 3e). Below 4000 m, $NDVI_{GS}$ velocity showed large fluctuations between about –87 and about 41 m/year. Above 4000 m, $NDVI_{GS}$ velocity decreased with elevation, remaining no more than 5 m/year away from zero, until the two highest bins.

We also investigated the sensitivity of vertical movements of $NDVI_{GS}$ isolines to temperature changes (Fig. 3f). The sensitivity fluctuated substantially between about –580 m/°C and about 391 m/°C in the bins below 3500 m, decreased sharply to about 58 m/°C at 3800 m, increased to about 146 m/°C at 4000 m, decreased steadily to about –136 m/°C at 5300 m, and increased to about –41 m/°C at 5700 m. In general, vertical movements of $NDVI_{GS}$ isolines were more sensitive to temperature changes below 4000 m and between 5200 and 5500 m. For their part, T_{GS} isolines rose with increased temperatures in all elevation bins. The sensitivity of these movements to temperature was slightly greater in the higher elevations, ranging from about 200 m/°C to about 380 m/°C, plus strong peaks around 4700 m and at 5200 and 5300 m. The sensitivity of T_{GS} isoline movements to temperature changes was in general 1 to 3 times that of $NDVI_{GS}$.

Spatial pattern of velocity of $NDVI_{GS}$ isoline movements

In addition to analyzing the data in terms of elevation bins, we examined the spatial pattern of variables, including the elevational gradient and temporal trend of $NDVI_{GS}$, and the velocity of vertical movements of $NDVI_{GS}$ isolines. The $NDVI_{GS}$ elevational gradient was negative in about 62% of pixels, mostly in the eastern and southern parts of the plateau, and positive in the remainder, mostly in the west, where the slopes were gentler (Fig. 4a). $NDVI_{GS}$ increased in 57% of pixels over the study period, mainly in the eastern and north-central parts of the plateau where temperature increased substantially, and decreased mostly in the western half, east of the center, and along the eastern edge of the plateau although most of those areas experienced increasing temperature (Fig. 4b, c).

The velocity of vertical movements of $\mathrm{NDVI_{GS}}$ isolines were spatially diverse (Fig. 4d), with a spatial standard deviation of 878 m/year. Both upward and downward movements of $\mathrm{NDVI_{GS}}$ isolines occurred all over the plateau. In general, the velocities of isoline movements were higher in the northeast, southeast, and south. In the eastern half of the plateau, upward movements of $\mathrm{NDVI_{GS}}$ isolines predominated over downward movements. Movements were upward in 53% of pixels. In about 49% of pixels, the velocity of these movements was within 5 m/year of zero, 24% being downward and 25% being upward

We also mapped the sensitivity of $\mathrm{NDVI_{GS}}$ isoline movements to temperature, which was spatially highly heterogeneous as it was with the velocity of isoline movements (Fig. 4e). Sensitivities were higher in the mountainous areas of the study area in the northeast, southeast, and south, and lower in the center and northwest where the terrain is flatter. A slight majority of pixels (52%) showed upward movements of $\mathrm{NDVI_{GS}}$ in response to temperature increase, meaning that in 48% of pixels $\mathrm{NDVI_{GS}}$ isolines tended to move downward as temperature increased.

The method predicts that temporally increasing $\mathrm{NDVI_{GS}}$ could result in $\mathrm{NDVI_{GS}}$ isolines moving either uphill or downhill. Our analysis, presented in Fig. 5a, found that in the 62% of pixels where the multiyear average of $\mathrm{NDVI_{GS}}$ decreased with elevation (negative elevational gradient), $\mathrm{NDVI_{GS}}$ isolines moved upward as $\mathrm{NDVI_{GS}}$ increased during the study period in 34% (blue points in Fig. 5a, mostly in the east) and downward in 28% (red points, mainly in the southwest and center). In the remaining 38% of pixels where the multiyear average of $NDVI_{GS}$ increased with elevation (positive elevational gradient), $NDVI_{GS}$ isolines moved upward as $NDVI_{GS}$ increased in 18% (green points, mostly in the west) and downward in 20% (orange points, no predominant location). The sensitivity of $NDVI_{GS}$ movements to temperature also showed similar direction along elevation, except for that there were more uphill movements in the center and more downhill movements of $NDVI_{GS}$ in the southeastern regions of the plateau in responses to higher temperature (Fig. 5b) compared with the $NDVI_{GS}$ velocity.

Relationship of $NDVI_{GS}$ isoline movement to slope and aspect

The elevational gradient of $NDVI_{GS}$ was lower in mountainous areas than in flatter areas, which suggests that terrain may affect the vertical movements of $NDVI_{GS}$ isolines. We found that 42% of pixels had slope angles greater than 15°, mostly in the southeast, the eastern and northeastern margins, and the south (Fig. 6a). Elsewhere the slope angles were less than 15°, particularly in the center and west where they were mostly less than 10°. The aspect showed no clear spatial patterns other than a direct relation to local topography, as expected (Fig. 6b).

The magnitude (both positive and negative) of the elevational gradient of $NDVI_{GS}$ decreased inversely with slope (Fig. 7a) and showed little variation with aspect (Fig. 8a). The positive temporal trend of $NDVI_{GS}$ was stable with respect to aspect for slope angles less than 37° but scattered at larger slope angles, whereas the negative $NDVI_{GS}$ trend gradually strengthened with slope angle and was more scattered with respect to aspect (Fig. 7b). The differences in the trend of $\mathrm{NDVI}_{\mathrm{GS}}$ at the same slope angle were associated with aspect (Fig. 8b). The velocity of vertical $\mathrm{NDVI}_{\mathrm{GS}}$ movements increased with slope angle (Fig. 7c) and strongly favored aspects of 135° and 315° (Fig. 8c). The sensitivity of $\mathrm{NDVI}_{\mathrm{GS}}$ isoline movements to temperature rise also increased with slope, except for the aspect of 315° (Fig. 7d). The sensitivity with positive value was greatest at the aspect of 315° whereas the sensitivity with negative value varied little with aspect (Fig. 8d).

Variability in vertical movements of $\mathrm{NDVI}_{\mathrm{GS}}$ isolines in relation to vegetation type

The elevational gradient of $\mathrm{NDVI}_{\mathrm{GS}}$ was greatest for cushion vegetation (about 0.6/km), followed in decreasing order by meadow, steppe, shrubland, and forest (Fig. 9a). This was true for both positive and negative values of gradient. In contrast, the temporal trend of $\mathrm{NDVI}_{\mathrm{GS}}$ showed little variation among the vegetation types and was stronger for positive gradients (15–20 10^{-4}/year) than for negative ones (11–16 10^{-4}/year) (Fig. 9b). As a consequence, forest had the highest vertical velocity, followed by shrubland, meadow, steppe, and cushion vegetation (Fig. 9c). The sensitivity of $\mathrm{NDVI}_{\mathrm{GS}}$ isoline movements to temperature change, both positive and negative, was also greatest for forest, then shrubland (Fig. 9d).

Discussion

Match and mismatch of elevational movements of T_{GS} and $NDVI_{GS}$ isolines

Our results confirmed that climate warming has caused substantial upward shifts in T_{GS} isolines on the Tibetan Plateau; however, the vertical shifts of $NDVI_{GS}$ isolines did not always match those of T_{GS} in either direction or magnitude (Fig. 3e). Mismatches were associated with the temporal trends and the elevational gradient of vegetation greenness. Downward shifts of greenness isolines were caused by either temporal decreases in greenness for elevation bins (or pixels) with negative $NDVI_{GS}$ elevational gradients or temporal increases in greenness for elevation bins (or pixels) with positive $NDVI_{GS}$ elevational gradients (Fig. 3e, 5). In the areas with positive $NDVI_{GS}$ elevational gradients, precipitation may increase with elevation (Wang *et al.*, 2013), resulting in higher greenness at higher elevation. Temporally increasing greenness will induce downshift of the greenness isolines. On the hand, downshift of the greenness isolines in the areas with negative $NDVI_{GS}$ elevational gradients should be caused by temporal decreases in greenness for which reason are given later. The lower speed of uphill shifts of greenness isolines compared with that of temperature isolines was because the ratio of $NDVI_{GS}$ trend to $NDVI_{GS}$ elevational gradient was lower than the ratio of T_{GS} trend to T_{GS} elevational gradient.

It is of interest to determine whether vertical shifts in greenness isolines were caused by the response of greenness to interannual variations in temperature on the Tibetan Plateau, where greenness is limited mainly by temperature (Shen *et al.*, 2015b, Wang *et al.*, 2015b, Wang *et al.*, 2012, Xu *et al.*, 2011). The consistency in sign between the sensitivity of $NDVI_{GS}$ isoline shifts to temperature and the velocity of $\mathrm{NDVI}_{\mathrm{GS}}$ isoline shifts suggests that the response of greenness to inter-annual variations in temperature played a determinative role in the direction of the elevational shifts of greenness isolines. Therefore, for the areas where increasing greenness shifts greenness isolines upward (i.e. where the $\mathrm{NDVI}_{\mathrm{GS}}$ elevational gradient is negative), represented by 62% of the pixels (Fig. 5a), the lag of uphill shifts of greenness isolines behind temperature isolines should reflect a lagging response of greenness to increasing temperature, and downhill shifts of greenness should reflect a negative impact of temperature on greenness.

The lagging response of and decrease in greenness may have several causes. First, the impacts of higher growing season temperature on vegetation growth are regulated by precipitation on the Tibetan Plateau. Low precipitation may weaken the positive impact of temperature, and continuous low water availability may even depress growth (Cong *et al.*, 2017, Liang *et al.*, 2012, Liang *et al.*, 2009, Lu *et al.*, 2018, Shen *et al.*, 2015a, Shen *et al.*, 2015b, Zhong *et al.*, 2010). Warming-enhanced evaporation may affect water availability (Gao *et al.*, 2015). Meanwhile, the degradation of permafrost induced by warming may also reduce soil water availability by deepening the active layer and thus enhancing the loss of soil water (Jin *et al.*, 2009, Qin *et al.*, 2017, Yi *et al.*, 2014). Water availability is a major determinant of vertical plant migration in arid and semiarid areas (Crimmins *et al.*, 2011). Second, climate warming may increase plants’ demands for nitrogen or other resources on the Tibetan Plateau (Liu *et al.*, 2015), which could restrict the effect of higher temperature on vegetation growth. Nutrition limitations are a key factor that prevents uphill movement of species under climate warming (Rumpf *et al.*, 2018). Third, another environmental factor such as CO_2 fertilization may also affect vegetation growth, but relevant observations are lacking for the Tibetan Plateau (Zhu *et al.*, 2016). Other possibilities include a decrease in sunshine duration, which could suppress vegetation growth (Wang *et al.*, 2015b), and spring warming, which may enhance greenness in spring and early summer by advancing the start of the growing season (Shen *et al.*, 2015c). Fourth, decreasing grazing pressure during the past decade may have contributed to greenness (Chen *et al.*, 2014). Fifth, temperature has increased rapidly, by about 0.4 °C per decade, during the past few decades on the plateau (Dong *et al.*, 2012, Duan & Xiao, 2015). Vegetation growth may have to some extent acclimated to this continuous rapid warming and become less responsive to recent temperature increases (Hikosaka *et al.*, 2006, Körner, 2007), although no evidence from the Tibetan Plateau has been published. Finally, climate change may have induced changes in the community's composition that affect overall greenness (Wang *et al.*, 2012). The impacts of climate change on community species composition and greenness and plant growth depend on elevation (Liu *et al.*, 2016), because many climatic factors are tied to elevation (Korner, 2007) . Moreover, vertical shifts in the distribution of species induced by climate change (Beckage *et al.*, 2008) should also have affected the shifts in greenness isolines. In addition, interactions between species may also affect vertical greenness shifts through their influence on species composition (Steinbauer *et al.*, 2018). Field observations across the plateau show that warming-induced upward shifts of treelines and shrublines were slowed by species interactions (Liang *et al.*, 2016, Wang *et al.*, 2015c, Wang *et al.*, 2016), providing direct evidence that inter- and intra-species could impact elevational movement of species distribution. A study in the Himalayas also suggests that the responses of plant species to climate change will not be unidirectional upward range shifts (Dolezal *et al.*, 2016). However, most of those studies are based on shrubs and trees, little is known about recent vertical shifts in herbaceous species distribution and their relation to climate change on the Tibetan Plateau. Intensive efforts will be required to disentangle the multiple abiotic and biotic factors affecting species distribution and greenness isolines on the Tibetan Plateau. Based on our current knowledge and the fact that most areas of the Tibetan Plateau are arid or semi-arid, it is likely that the limitation in water availability would be the most feasible cause of the lagging response of greenness to warming.

The Tibetan Plateau is recognized as an important terrestrial carbon pool (Piao *et al.*, 2009). Because greenness is a direct indicator of an ecosystem's primary production, the lag of greenness isolines behind temperature isolines suggests that the sensitivity of primary carbon uptake by the ecosystem to temperature is decreasing. Such a decrease could reduce the net carbon uptake of the Tibetan Plateau ecosystem, because ecosystem respiration increases exponentially with temperature (Lin *et al.*, 2011). It is even possible that the plateau will change from a carbon pool to a carbon source in the feature (Tan *et al.*, 2010). Realistic process-based models for the plateau ecosystem are needed to identify the climate conditions under which that transition might occur.

Terrain effects on the elevational shifts of greenness isolines

Besides the temporal response of $NDVI_{GS}$ to climate change and other factors, the velocity of $NDVI_{GS}$ isoline movements is determined by the $NDVI_{GS}$ elevational gradient as shown in Fig. 3e, f. We found that the slope angle of a pixel, when less than 15°, strongly affected the magnitude of the $NDVI_{GS}$ elevational gradient and thus the vertical velocity of $NDVI_{GS}$ and its sensitivity to temperature. Vertical shifts of $NDVI_{GS}$ isolines were faster and more sensitive to temperature where the slope angle was greater than 15°, because steeper slopes resulted in smaller $NDVI_{GS}$ elevational gradients. The role of slope may be connected to vegetation types, because on the Tibetan Plateau forests are in areas with the steepest slopes, followed by shrubland, cushion vegetation, steppe, and meadow. The dominant role of slope in determining the $NDVI_{GS}$ elevational gradient could be possibly because $NDVI_{GS}$ was not sensitive to slope angle at slopes gentler than 15°. In contrast, the impacts of aspect were small. Those results highlight the impact of slope angle on vertical shifts of $NDVI_{GS}$ isolines. There is a need to explore the role of terrain effects in regulating the responses to climate warming of species distribution and population dynamics, a topic that has attracted little attention (Gottfried *et al.*, 1999, Jackson *et al.*, 2016). Geomorphic factors were paid more attentions than terrain effects (Macias-Fauria & Johnson, 2013).

limitations and future prospects

Obviously, the elevational gradients of $NDVI_{GS}$ and T_{GS} are dependent on the spatial resolution of the grid, as are the speed of vertical shifts of $NDVI_{GS}$ and the sensitivity of that speed to temperature. The coarse spatial resolution of the grid may limit our insights into the elevational gradients and elevational shifts. In particular, there is no gridded climate data with fine resolution available. Although we used 0.1° × 0.1° climate data, the finest resolution available, the resolution was still too coarse to investigate the spatial pattern of T_{GS} isoline movements. On the other hand, the fine resolution remotely sensed vegetation greenness data suffered from low temporal resolution, contamination by clouds, and poor spatial coverage. High-accuracy methods are needed for blending imagery of fine and coarse resolution in areas of rugged topography on the Tibetan Plateau and elsewhere. Long-term in situ observations of meteorological conditions, population dynamics and community composition could usefully be established along representative elevational gradients on the plateau.

In summary, we investigated the vertical shifts of vegetation greenness and temperature in the context of climate warming on the Tibetan Plateau. We found that greenness and temperature isolines moved at different rates. We speculate that the lagging response of greenness to interannual temperature changes may be related to water limitation and the elevational gradient of greenness. The vertical gradient of greenness, variation of which is strongly determined by slope angle, further explained the spatial variations in the vertical velocity of greenness isolines and the sensitivity of these vertical movements to temporal temperature changes, highlighting the role of terrain effects on vertical shifts of greenness. The lagging response of greenness to temperature may weaken carbon sequestration by Tibetan Plateau ecosystems, given that greenness is an indicator of primary carbon uptake and ecosystem respiration increases exponentially with temperature. Our study suggests that further multiple-scale studies are needed to clarify the ecological processes that may affect vertical shifts in species distribution and greenness isolines on the Tibetan Plateau.

Acknowledgments

This work was funded by Key Research and Development Programs for Global Change and Adaptation (Grant No. 2017YFA0603604), the Key Research Program of Frontier Sciences and Strategic Priority Research Program (A) of the Chinese Academy of Sciences (Grants No. QYZDB-SSW-DQC025 and XDA20050101), the National Natural Science Foundation of China (Grants No. 41571103 and 41701378), Top-Notch Young Talents Program of China (to Shen), and the Youth Innovation Promotion Association of the Chinese Academy of Sciences (Grant No. 2015055). The authors declare no conflict of interest.

References

Alexander JM, Chalmandrier L, Lenoir J *et al.* (2018) Lags in the response of mountain plant communities to climate change. Global Change Biology, **24**, 563-579.

Beckage B, Osborne B, Gavin DG, Pucko C, Siccama T, Perkins T (2008) A rapid upward shift of a forest ecotone during 40 years of warming in the Green Mountains of Vermont. Proceedings of the National Academy of Sciences, **105**, 4197-4202.

Bertrand R, Lenoir J, Piedallu C *et al.* (2011) Changes in plant community composition lag behind climate warming in lowland forests. Nature, **479**, 517-520.

Bibi S, Wang L, Li X, Zhou J, Chen D, Yao T (2018) Climatic and associated cryospheric, biospheric, and hydrological changes on the Tibetan Plateau: a review. International Journal of Climatology, n/a-n/a.

Chen BX, Zhang XZ, Tao J *et al.* (2014) The impact of climate change and anthropogenic activities on alpine grassland over the Qinghai-Tibet Plateau. Agricultural and Forest Meteorology, **189**, 11-18.

Chen Y, Yang K, He J, Qin J, Shi J, Du J, He Q (2011) Improving land surface temperature modeling for dry land of China. Journal of Geophysical Research, **116**, doi: 10.1029/2011jd015921.

Cong N, Shen M, Yang W, Yang Z, Zhang G, Piao S (2017) Varying responses of vegetation activity to climate changes on the Tibetan Plateau grassland. Int J Biometeorol, **61**, 1433–1444

Crimmins SM, Dobrowski SZ, Greenberg JA, Abatzoglou JT, Mynsberge AR (2011) Changes in climatic water balance drive downhill shifts in plant species' optimum elevations. Science, **331**, 324-327.

Didan K, Munoz A, Solano R, Huete A (2015) MODIS Vegetation Index User's Guide (MOD13 Series) Version 3.00 (Collection 6). pp Page.

Dolezal J, Dvorsky M, Kopecky M *et al.* (2016) Vegetation dynamics at the upper elevational limit of vascular plants in Himalaya. Sci Rep, **6**, 24881.

Dong M, Jiang Y, Zheng C, Zhang D (2012) Trends in the thermal growing season throughout the Tibetan Plateau during 1960–2009. Agricultural and Forest Meteorology, **166-167**, 201-206.

Dorji T, Totland O, Moe SR, Hopping KA, Pan J, Klein JA (2013) Plant functional traits mediate reproductive phenology and success in response to experimental warming and snow addition in Tibet. Global Change Biology, **19**, 459-472.

Duan A, Xiao Z (2015) Does the climate warming hiatus exist over the Tibetan Plateau? Sci Rep, **5**, 13711.

Edwards R, Treitz P (2017) Vegetation greening trends at two sites in the Canadian Arctic: 1984-2015. Arctic Antarctic and Alpine Research, **49**, 601-619.

Gao YH, Li X, Leung LR, Chen DL, Xu JW (2015) Aridity changes in the Tibetan Plateau in a warming climate. Environmental Research Letters, **10**, doi: 10.1088/1748-9326/1010/1083/034013.

Geng Y, Wang Y, Yang K *et al.* (2012) Soil respiration in Tibetan alpine grasslands: belowground biomass and soil moisture, but not soil temperature, best explain the large-scale patterns. PLoS One, **7**, e34968.

Gottfried M, Pauli H, Futschik A *et al.* (2012) Continent-wide response of mountain vegetation to climate change. Nature Climate Change, **2**, 111-115.

Gottfried M, Pauli H, Reiter K, Grabherr G (1999) A fine ‐ scaled predictive model for changes in species distribution patterns of high mountain plants induced by climate warming. Diversity and Distributions, **5**, 241-251.

Guay KC, Beck PSA, Berner LT, Goetz SJ, Baccini A, Buermann W (2014) Vegetation productivity patterns at high northern latitudes: a multi-sensor satellite data assessment. Global Change Biology, **20**, 3147-3158.

He J (2010) Development of surface meteorological dataset of China with high temporal and spatial resolution. Unpublished M. S. Chin. Acad. of Sci.,, Beijing, China.

Hikosaka K, Ishikawa K, Borjigidai A, Muller O, Onoda Y (2006) Temperature acclimation of photosynthesis: mechanisms involved in the changes in temperature dependence of photosynthetic rate. J Exp Bot, **57**, 291-302.

Huete A, Didan K, Miura T, Rodriguez EP, Gao X, Ferreira LG (2002) Overview of the radiometric and biophysical performance of the MODIS vegetation indices. Remote Sensing of Environment, **83**, 195-213.

Huffman GJ, Adler RF, Bolvin DT *et al.* (2007) The TRMM multisatellite precipitation analysis (TMPA): Quasi-global, multiyear, combined-sensor precipitation estimates at fine scales. Journal of Hydrometeorology, **8**, 38-55.

Jackson MM, Topp E, Gergel SE, Martin K, Pirotti F, Sitzia T (2016) Expansion of subalpine woody vegetation over 40 years on Vancouver Island, British Columbia, Canada. Canadian Journal of Forest Research, **46**, 437-443.

Jin H, He R, Cheng G, Wu Q, Wang S, Lü L, Chang X (2009) Changes in frozen ground in the Source Area of the Yellow River on the Qinghai–Tibet Plateau, China, and their eco-environmental impacts. Environmental Research Letters, **4**, 045206.

Klanderud K, Birks HJB (2003) Recent increases in species richness and shifts in altitudinal distributions of Norwegian mountain plants. Holocene, **13**, 1-6.

Korner C (2007) The use of 'altitude' in ecological research. Trends Ecol Evol, **22**, 569-574.

Körner C (2003) *Alpine plant life-Functional plant ecology of high mountain ecosystems,* Heidelberg, Springer.

Körner C (2007) Significance of Temperature in Plant Life. In: *Plant Growth and Climate Change.* (ed J.I.L. M) pp Page., Blackwell Publishing Ltd.

Lenoir J, Gegout JC, Marquet PA, De Ruffray P, Brisse H (2008) A significant upward shift in plant species optimum elevation during the 20th century. Science, **320**, 1768-1771.

Liang E, Lu X, Ren P, Li X, Zhu L, Eckstein D (2012) Annual increments of juniper dwarf shrubs above the tree line on the central Tibetan Plateau: a useful climatic proxy. Ann Bot, **109**, 721-728.

Liang E, Wang Y, Piao S *et al.* (2016) Species interactions slow warming-induced upward shifts of treelines on the Tibetan Plateau. Proc Natl Acad Sci U S A, **113**, 4380-4385.

Liang EY, Shao XM, Xu Y (2009) Tree-ring evidence of recent abnormal warming on the southeast Tibetan Plateau. Theor Appl Climatol, **98**, 9-18.

Lin X, Zhang Z, Wang S *et al.* (2011) Response of ecosystem respiration to warming and grazing during the growing seasons in the alpine meadow on the Tibetan plateau. Agricultural and Forest Meteorology, **151**, 792-802.

Liu B, Wang Y, Zhu H, Liang E, Camarero JJ (2016) Topography and age mediate the growth responses of Smith fir to climate warming in the southeastern Tibetan Plateau. Int J Biometeorol, **60**, 1577–1587

Liu YW, Xu R, Wang YS, Pan YP, Piao SL (2015) Wet deposition of atmospheric inorganic nitrogen at five remote sites in the Tibetan Plateau. Atmos. Chem. Phys., **15**, 11683-11700.

Lu X, Huang R, Wang Y, Sigdel SR, Dawadi B, Liang E, Camarero JJ (2018) Summer Temperature Drives Radial Growth of Alpine Shrub Willows on the Northeastern Tibetan Plateau. Arctic, Antarctic, and Alpine Research, **48**, 461-468.

Macias-Fauria M, Johnson EA (2013) Warming-induced upslope advance of subalpine forest is severely limited by geomorphic processes. Proc Natl Acad Sci U S A, **110**, 8117-8122.

Mountain-Research-Initiative-Edw-Working-Group (2015) Elevation-dependent warming in mountain regions of the world. Nature Clim. Change, **5**, 424-430.

Myneni RB, Keeling CD, Tucker CJ, Asrar G, Nemani RR (1997) Increased plant growth in the northern high latitudes from 1981 to 1991. Nature, **386**, 698-702.

Piao S, Tan K, Nan H *et al.* (2012) Impacts of climate and CO2 changes on the vegetation growth and carbon balance of Qinghai–Tibetan grasslands over the past five decades. Global and Planetary Change, **98-99**, 73-80.

Piao SL, Fang JY, Ciais P, Peylin P, Huang Y, Sitch S, Wang T (2009) The carbon balance of terrestrial ecosystems in China. Nature, **458**, 1009-1014.

Qin Y, Yang DW, Gao B *et al.* (2017) Impacts of climate warming on the frozen ground and eco-hydrology in the Yellow River source region, China. Science of the Total Environment, **605**, 830-841.

Rumpf SB, Hulber K, Klonner G *et al.* (2018) Range dynamics of mountain plants decrease with elevation. Proc Natl Acad Sci U S A, **115**, 1848-1853.

Saikkonen K, Taulavuori K, Hyvonen T *et al.* (2012) Climate change-driven species' range shifts filtered by photoperiodism. Nature Climate Change, **2**, 239-242.

Sheffield J, Goteti G, Wood EF (2006) Development of a 50-year high-resolution global dataset of meteorological forcings for land surface modeling. Journal of Climate, **19**, 3088-3111.

Shen M, Piao S, Cong N, Zhang G, Jassens IA (2015a) Precipitation impacts on vegetation spring phenology on the Tibetan Plateau. Global Change Biology, **21**, 3647-3656.

Shen M, Piao S, Jeong SJ *et al.* (2015b) Evaporative cooling over the Tibetan Plateau induced by vegetation growth. Proceedings of the National Academy of Sciences USA, **112**, 9299-9304.

Shen M, Piao SL, Dorji T *et al.* (2015c) Plant phenological responses to climate change on the Tibetan Plateau: research status and challenges. National Science Review, **22**, 454-467.

Shen M, Tang Y, Klein J, Zhang P, Gu S, Shimono A, Chen J (2008) Estimation of aboveground biomass using in situ hyperspectral measurements in five major grassland ecosystems on the Tibetan Plateau. Journal of Plant Ecology, **1**, 247-257.

Shen M, Zhang G, Cong N, Wang S, Kong W, Piao S (2014) Increasing altitudinal gradient of spring vegetation phenology during the last decade on the Qinghai–Tibetan Plateau. Agricultural and Forest Meteorology, **189-190**, 71-80.

Steinbauer MJ, Grytnes J-A, Jurasinski G *et al.* (2018) Accelerated increase in plant species richness on mountain summits is linked to warming. Nature, **556**, 231-234.

Tan K, Ciais P, Piao S *et al.* (2010) Application of the ORCHIDEE global vegetation model to evaluate biomass and soil carbon stocks of Qinghai-Tibetan grasslands. Global Biogeochemical Cycles, **24**, doi: 10.1029/2009gb003530.

Tao J, Zhang Y, Dong J *et al.* (2015) Elevation-dependent relationships between climate change and grassland vegetation variation across the Qinghai-Xizang Plateau. International Journal of Climatology, **35**, 1638-1647.

Tucker CJ, Fung IY, Keeling CD, Gammon RH (1986) Relationship between atmospheric CO2 variations and a satellite-derived vegetation index. Nature, **319**, 195-199.

Wang CZ, Guo HD, Zhang L, Liu SY, Qiu YB, Sun ZC (2015a) Assessing phenological change and climatic control of alpine grasslands in the Tibetan Plateau with MODIS time series. Int J Biometeorol, **59**, 11-23.

Wang H, Liu D, Lin H, Montenegro A, Zhu X (2015b) NDVI and vegetation phenology dynamics under the influence of sunshine duration on the Tibetan plateau. International Journal of Climatology, **35**, 687-698.

Wang S, Duan J, Xu G *et al.* (2012) Effects of warming and grazing on soil N availability, species composition, and ANPP in an alpine meadow. Ecology, **93**, 2365-2376.

Wang Y, Liang E, M Ellison A, Xiaoming L, Camarero J (2015c) Facilitation stabilizes moisture-controlled alpine juniper shrublines in the central Tibetan Plateau. **132**, 20–30.

Wang Y, Pederson N, Ellison AM, Buckley HL, Case BS, Liang E, Camarero JJ (2016) Increased stem density and competition may diminish the positive effects of warming at alpine treeline. Ecology, **97**, 1668–1679.

Wang Z, Luo T, Li R, Tang Y, Du M (2013) Causes for the unimodal pattern of biomass and productivity in alpine grasslands along a large altitudinal gradient in semi-arid regions. Journal of Vegetation Science, **24**, 189-201.

Wu G, Liu Y (2016) Impacts of the Tibetan Plateau on Asian Climate. Meteorological Monographs, **56**, 7.1-7.29.

Wu GX, Liu YM, He B, Bao Q, Duan AM, Jin FF (2012) Thermal Controls on the Asian Summer Monsoon. Sci Rep, **2**, doi: 10.1038/srep00404.

Xu L, Myneni RB, Chapin Iii FS *et al.* (2013) Temperature and vegetation seasonality diminishment over northern lands. Nat Clim Chang, **3**, 581-586.

Xu W, Gu S, Zhao X *et al.* (2011) High positive correlation between soil temperature and NDVI from 1982 to 2006 in alpine meadow of the Three-River Source Region on the Qinghai-Tibetan Plateau. International Journal of Applied Earth Observation and Geoinformation, **13**, 528-535.

Xu YM, Knudby A, Ho HC, Shen Y, Liu YH (2017) Warming over the Tibetan Plateau in the last 55 years based on area-weighted average temperature. Regional Environmental Change, **17**, 2339-2347.

Yatagai A, Arakawa O, Kamiguchi K, Kawamoto H, Nodzu MI, Hamada A (2009) A 44-Year Daily Gridded Precipitation Dataset for Asia Based on a Dense Network of Rain Gauges. Sola, **5**, 137-140.

Yi SH, Wang XY, Qin Y, Xiang B, Ding YJ (2014) Responses of alpine grassland on Qinghai-Tibetan plateau to climate warming and permafrost degradation: a modeling perspective. Environmental Research Letters, **9**, doi: 10.1088/1748-9326/1089/1087/074014.

Zhang J, Wu L, Huang G, Zhu W, Zhang Y (2011) The role of May vegetation greenness on the southeastern Tibetan Plateau for East Asian summer monsoon prediction. Journal of Geophysical Research, **116**, doi: 10.1029/2010JD015095.

Zhong L, Ma YM, Salama MS, Su ZB (2010) Assessment of vegetation dynamics and their response to variations in precipitation and temperature in the Tibetan Plateau. Climatic Change, **103**, 519-535.

Zhu ZC, Piao SL, Myneni RB *et al.* (2016) Greening of the Earth and its drivers. Nature Climate Change, **6**, 791-795.

Table 1 Definition of the direction of velocity of NDVI_{GS} isolines along elevation.

Elevational gradient of NDVI_{GS}	Temporal trend or sensitivity to temperature of NDVI_{GS}	Velocity of NDVI_{GS} movement
Negative (decreasing with elevation)	Positive	Positive (uphill)
Negative	Negative	Negative (downhill)
Positive (increasing with elevation)	Positive	Negative (downhill)
Positive	Negative	Positive (uphill)

Figure 1 Diagram showing the determination of the elevational gradient of NDVI_{GS} at the central pixel.

Figure 2 Dependence upon elevation of mean growing season temperature T_{GS} (a) and mean growing season greenness NDVI_{GS} (b) over the period 2000–2016. The points and error bars indicate mean values and standard deviations for each 100-m elevation bin.

Figure 3 Dependence upon elevation of the elevational gradient of T_{GS} (a) and NDVI_{GS} (b), the temporal trend of T_{GS} (c) and NDVI_{GS} (d), the velocity of vertical movements of T_{GS} and

$NDVI_{GS}$ isolines (e), and the sensitivity of vertical movements of $NDVI_{GS}$ and T_{GS} isolines to temperature (f). The circles in blacks indicate that the trends are significant at $P < 0.10$ level.

Figure 4 Spatial distribution of the elevational gradient (a) and temporal trend (b) of $NDVI_{GS}$, temporal trend of T_{GS} (c), the velocity of vertical movements of $NDVI_{GS}$ isolines (d), and the sensitivity of vertical movements of $NDVI_{GS}$ isolines to temperature (e). Top-middle insets in each plate show the proportion of pixels in each interval of the mapped variable, keyed by color to the legend at lower left. Top-right insets in (b) and (c) show $NDVI_{GS}$ increase (green) or decrease (red) and T_{GS} increase (red) or decrease (blue) at $P < 0.10$ level, respectively.

Figure 5 Spatial distribution of the vertical movement of $NDVI_{GS}$ isolines (a) and the sensitivity of vertical movements of $NDVI_{GS}$ isolines to temperature (b). Pixel colors express combinations of the signs of the elevational gradient of $NDVI_{GS}$ (AG), the temporal trend of $NDVI_{GS}$ (Trend), and the temperature sensitivity of $NDVI_{GS}$ (TS). Insets show the proportion of pixels with each combination.

Figure 6 Spatial distribution of slope angle (a) and aspect (b) on the Tibetan Plateau. Insets show the proportion of pixels in each interval of slope angle or aspect signified by the color key at lower left.

Figure 7 Variations with slope angle of the elevational gradient (a) and temporal trend (b) of $NDVI_{GS}$, the velocity of vertical movement of $NDVI_{GS}$ isolines (c), and the sensitivity of vertical movement of $NDVI_{GS}$ isolines to temperature (d). Colored curves represent the values in each 2.5° bin of slope angle for each of eight aspect azimuths. Positive and negative values were averaged separately.

Figure 8 Variations with aspect azimuth of the elevational gradient (a) and temporal trend (b) of $\mathrm{NDVI}_{\mathrm{GS}}$, the velocity of vertical movement of $\mathrm{NDVI}_{\mathrm{GS}}$ isolines (c), and the sensitivity of vertical movement of $\mathrm{NDVI}_{\mathrm{GS}}$ isolines to temperature (d). Colored curves and symbols represent mean values for each 5° slope bin (legend at right shows the central value of each bin). Positive and negative values were averaged separately.

Figure 9 Elevational gradient (a) and temporal trend (b) of $\mathrm{NDVI}_{\mathrm{GS}}$, velocity of vertical movement of $\mathrm{NDVI}_{\mathrm{GS}}$ isolines (c), and sensitivity of vertical movement of $\mathrm{NDVI}_{\mathrm{GS}}$ isolines to temperature (d) for five vegetation types on the Tibetan Plateau. Positive (blue) and negative (red) values were averaged separately, and the gray bars show overall mean for each vegetation type.

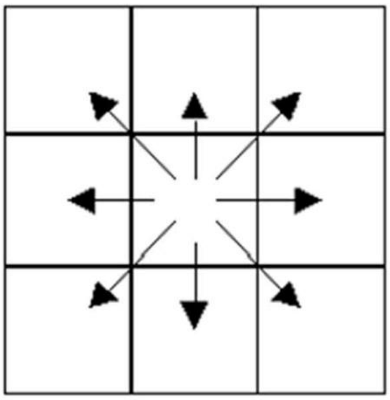

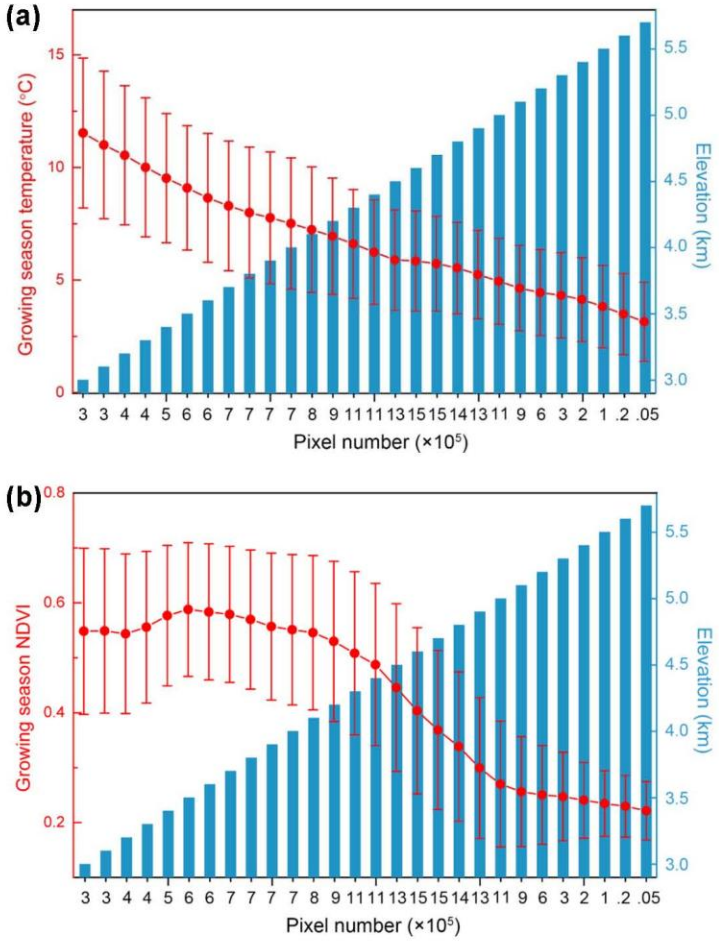
(a)
Growing season temperature (°C)
0
5
10
15
Elevation (km)
3.0
3.5
4.0
4.5
5.0
5.5
3 3 4 4 5 6 6 7 7 7 7 8 9 11 11 13 15 15 14 13 11 9 6 3 2 1 .2 .05
Pixel number (×10⁵)
(b)
Growing season NDVI
0.2
0.4
0.6
0.8
Elevation (km)
3.0
3.5
4.0
4.5
5.0
5.5
3 3 4 4 5 6 6 7 7 7 7 8 9 11 11 13 15 15 14 13 11 9 6 3 2 1 .2 .05
Pixel number (×10⁵)

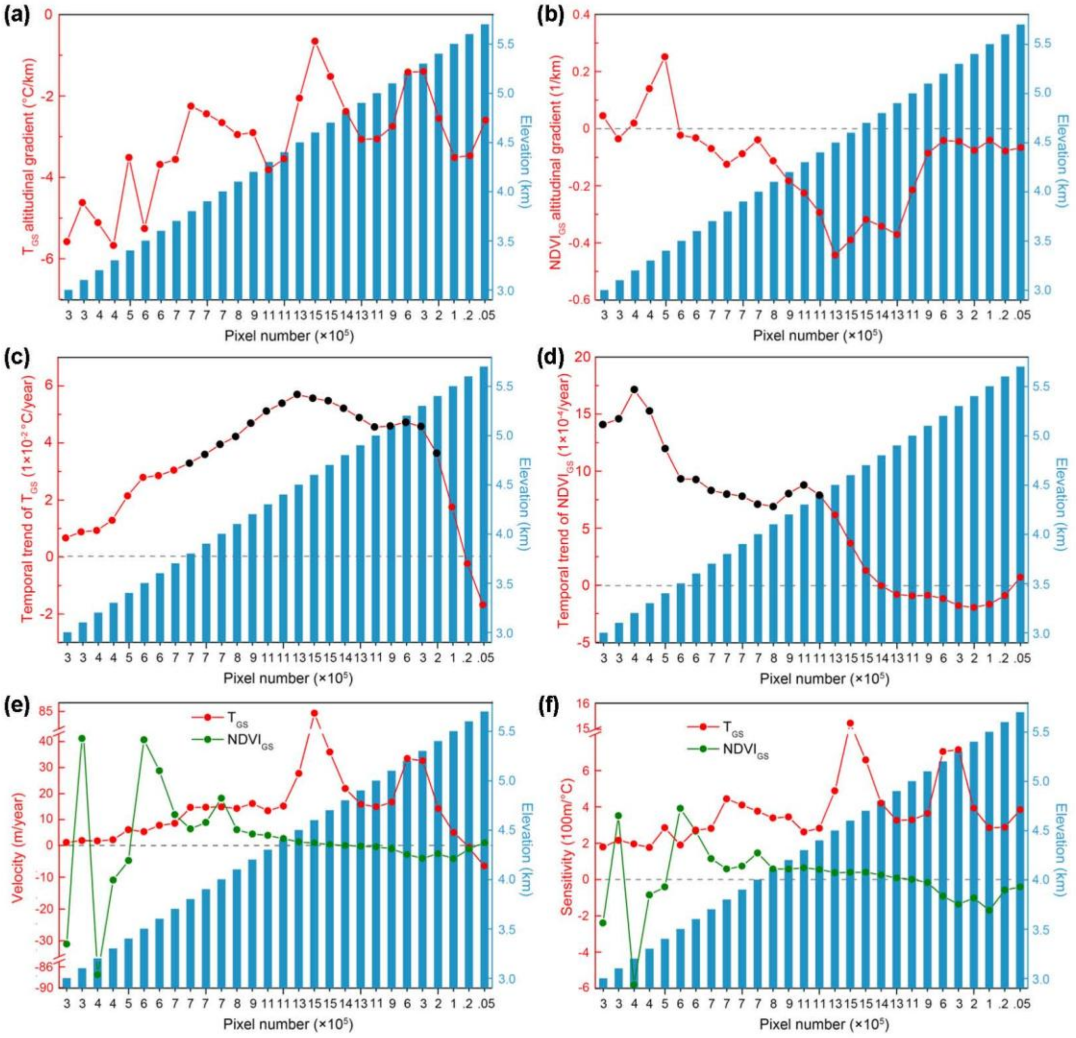
(a)
T$_{GS}$ altitudinal gradient (°C/km)
0
-2
-4
-6
Elevation (km)
3.0
3.5
4.0
4.5
5.0
5.5
Pixel number (×10^5)
3 3 4 4 5 6 6 7 7 7 7 8 9 11 11 11 13 15 15 14 13 11 9 6 3 2 1 .2 .05
(b)
NDVI$_{GS}$ altitudinal gradient (1/km)
0.4
0.2
0
-0.2
-0.4
-0.6
Elevation (km)
(c)
Temporal trend of T$_{GS}$ (1×10^{-2} °C/year)
6
4
2
0
-2
Elevation (km)
(d)
Temporal trend of NDVI$_{GS}$ (1×10^{-4}/year)
20
15
10
5
0
-5
Elevation (km)
(e)
T$_{GS}$
NDVI$_{GS}$
Velocity (m/year)
85
40
30
20
10
0
-10
-20
-30
-86
-90
Elevation (km)
(f)
T$_{GS}$
NDVI$_{GS}$
Sensitivity (100m/°C)
16
15
6
4
2
0
-2
-4
-6
Elevation (km)

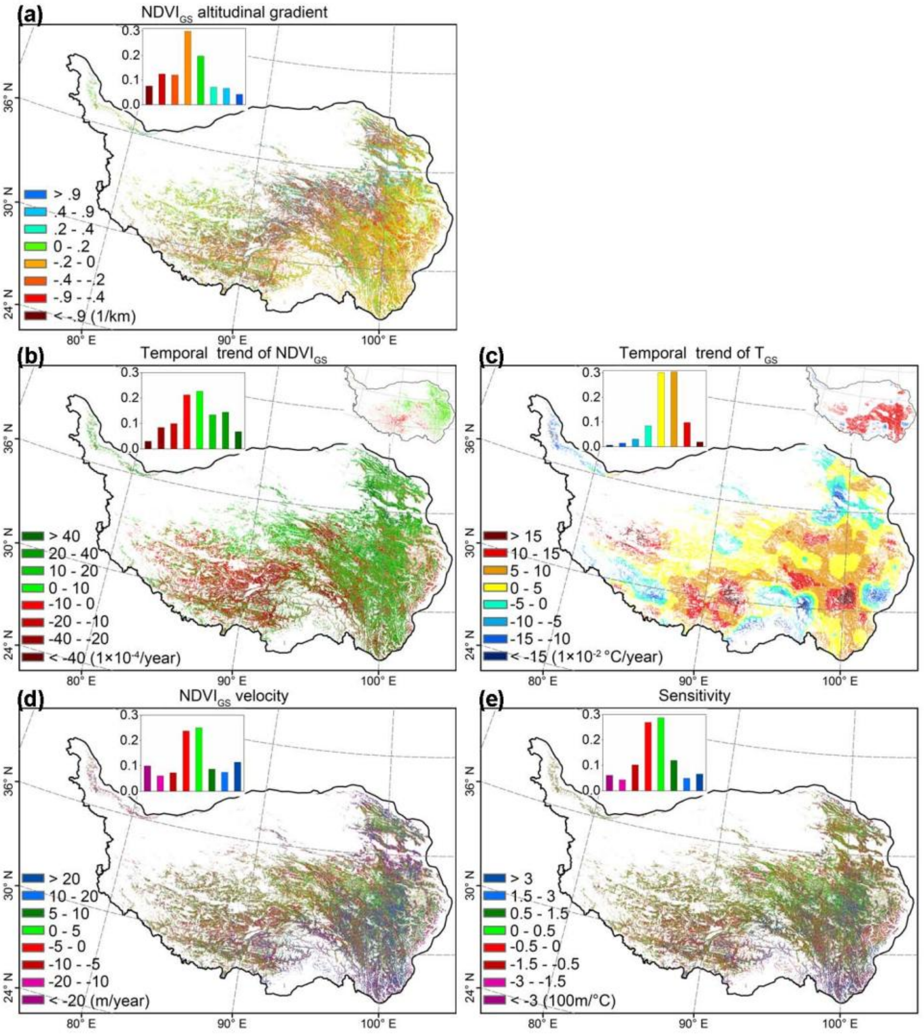
(a)
NDVI$_{GS}$ altitudinal gradient
> .9
.4 - .9
.2 - .4
0 - .2
-.2 - 0
-.4 - -.2
-.9 - -.4
< -.9 (1/km)
(b)
Temporal trend of NDVI$_{GS}$
> 40
20 - 40
10 - 20
0 - 10
-10 - 0
-20 - -10
-40 - -20
< -40 (1×10^{-4}/year)
(c)
Temporal trend of T$_{GS}$
> 15
10 - 15
5 - 10
0 - 5
-5 - 0
-10 - -5
-15 - -10
< -15 (1×10^{-2} °C/year)
(d)
NDVI$_{GS}$ velocity
> 20
10 - 20
5 - 10
0 - 5
-5 - 0
-10 - -5
-20 - -10
< -20 (m/year)
(e)
Sensitivity
> 3
1.5 - 3
0.5 - 1.5
0 - 0.5
-0.5 - 0
-1.5 - -0.5
-3 - -1.5
< -3 (100m/°C)
0.3
0.2
0.1
0.0
36° N
30° N
24° N
80° E
90° E
100° E

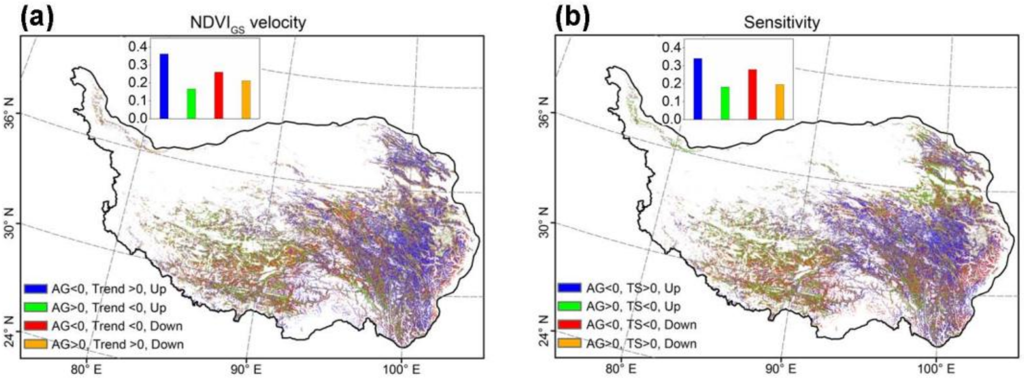
(a)
NDVI$_{GS}$ velocity
0.4
0.3
0.2
0.1
0.0
36° N
30° N
24° N
80° E
90° E
100° E
AG<0, Trend >0, Up
AG>0, Trend <0, Up
AG<0, Trend <0, Down
AG>0, Trend >0, Down
(b)
Sensitivity
0.4
0.3
0.2
0.1
0.0
36° N
30° N
24° N
80° E
90° E
100° E
AG<0, TS>0, Up
AG>0, TS<0, Up
AG<0, TS<0, Down
AG>0, TS>0, Down

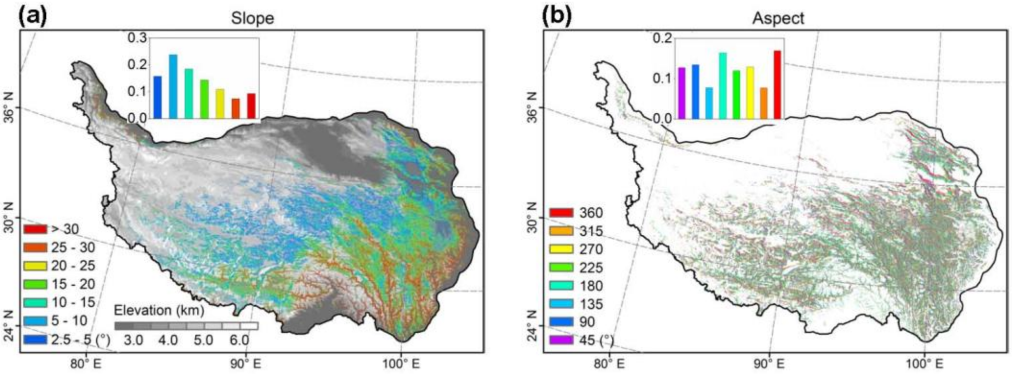
(a)
Slope
0.3
0.2
0.1
0.0
36° N
30° N
24° N
> 30
25 - 30
20 - 25
15 - 20
10 - 15
5 - 10
2.5 - 5 (°)
Elevation (km)
3.0
4.0
5.0
6.0
80° E
90° E
100° E
(b)
Aspect
0.2
0.1
0.0
36° N
30° N
24° N
360
315
270
225
180
135
90
45 (°)
80° E
90° E
100° E

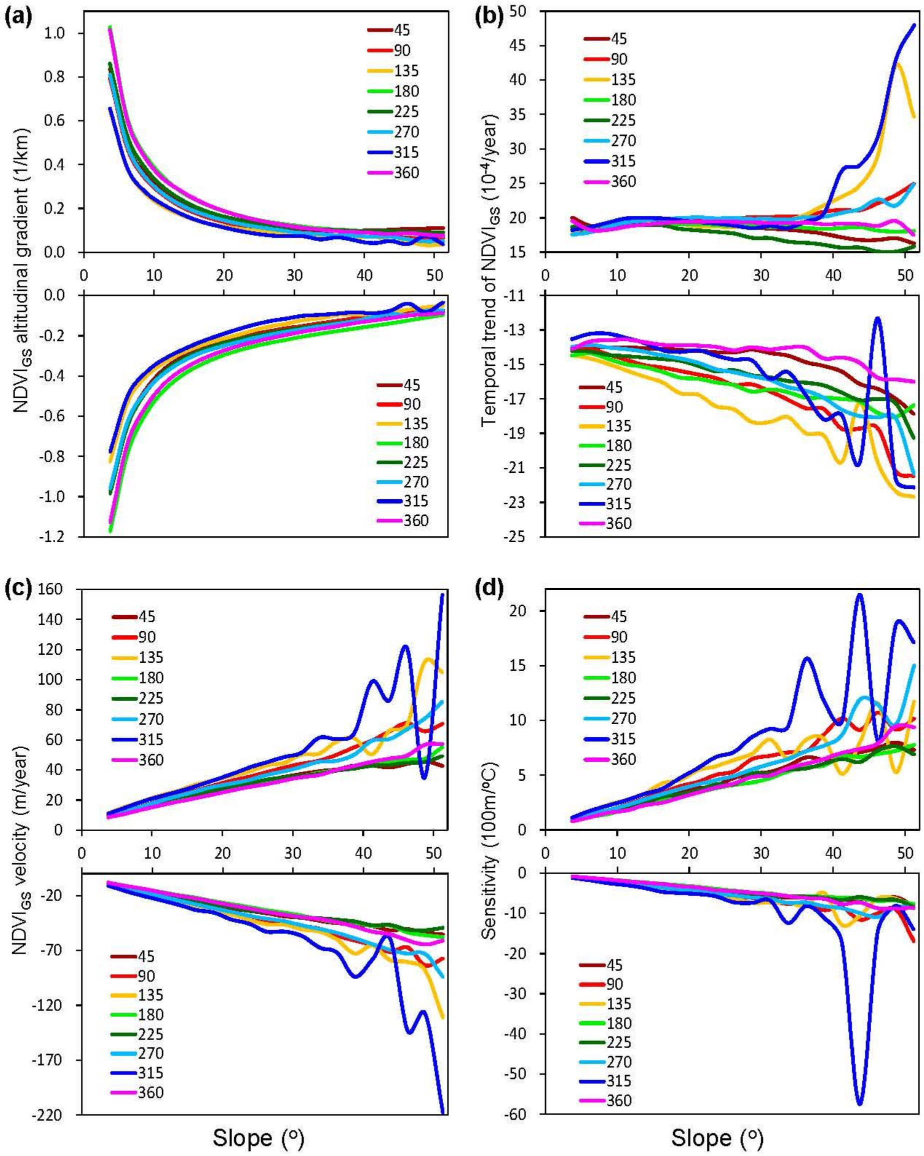
(a)
(b)
(c)
(d)
NDVI$_{GS}$ altitudinal gradient (1/km)
Temporal trend of NDVI$_{GS}$ (10^{-4}/year)
NDVI$_{GS}$ velocity (m/year)
Sensitivity (100m/ºC)
Slope (º)
Slope (º)
1.0
0.8
0.6
0.4
0.2
0.0
-0.2
-0.4
-0.6
-0.8
-1.0
-1.2
50
45
40
35
30
25
20
15
-11
-13
-15
-17
-19
-21
-23
-25
160
140
120
100
80
60
40
20
0
-20
-70
-120
-170
-220
10
5
-10
-30
-40
-50
-60
0
10
20
30
40
50
45
90
135
180
225
270
315
360

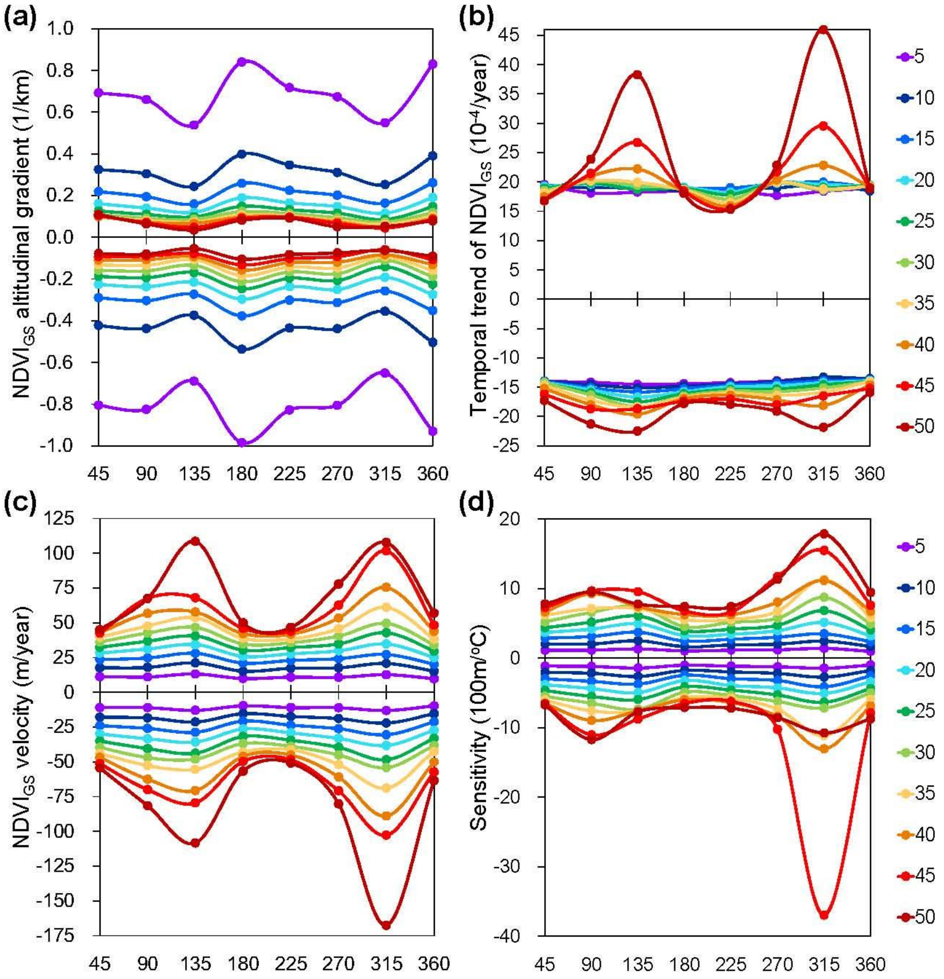
(a)
NDVI$_{GS}$ altitudinal gradient (1/km)
1.0
0.8
0.6
0.4
0.2
0.0
-0.2
-0.4
-0.6
-0.8
-1.0
45 90 135 180 225 270 315 360
(b)
Temporal trend of NDVI$_{GS}$ (10^{-4}/year)
45
40
35
30
25
20
15
10
5
0
-5
-10
-15
-20
-25
45 90 135 180 225 270 315 360
(c)
NDVI$_{GS}$ velocity (m/year)
125
100
75
50
25
0
-25
-50
-75
-100
-125
-150
-175
45 90 135 180 225 270 315 360
(d)
Sensitivity (100m/°C)
20
10
0
-10
-20
-30
-40
45 90 135 180 225 270 315 360
5
10
15
20
25
30
35
40
45
50
5
10
15
20
25
30
35
40
45
50

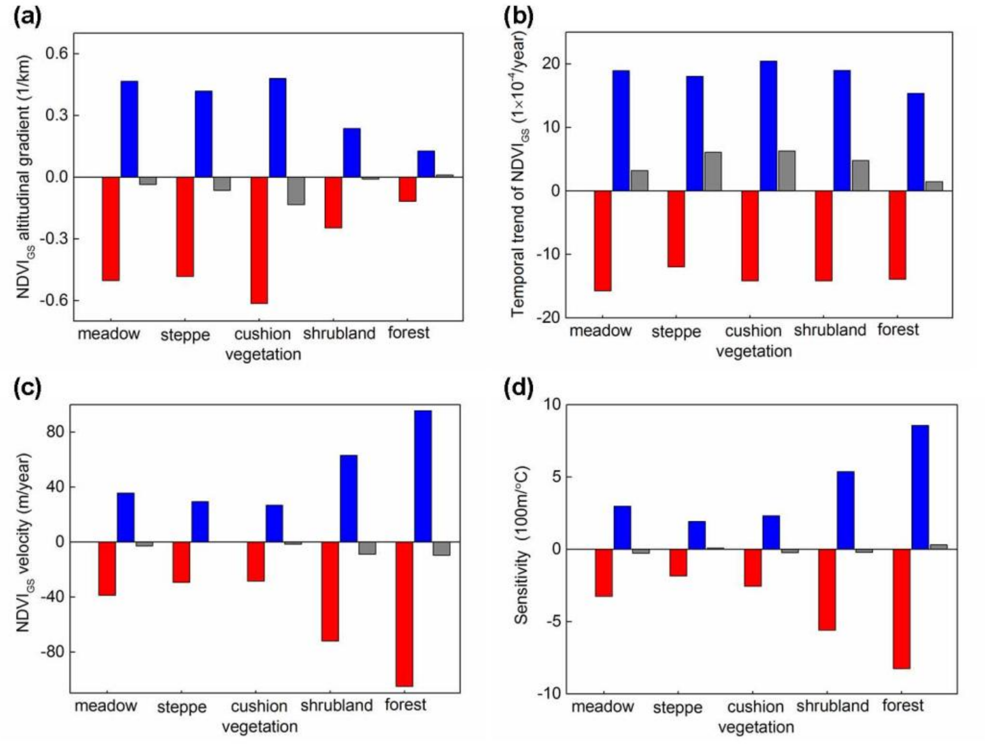
(a)
NDVI$_{GS}$ altitudinal gradient (1/km)
0.6
0.3
0.0
-0.3
-0.6
meadow
steppe
cushion
shrubland
forest
vegetation
(b)
Temporal trend of NDVI$_{GS}$ (1×10^{-4}/year)
20
10
0
-10
-20
meadow
steppe
cushion
shrubland
forest
vegetation
(c)
NDVI$_{GS}$ velocity (m/year)
80
40
0
-40
-80
meadow
steppe
cushion
shrubland
forest
vegetation
(d)
Sensitivity (100m/°C)
10
5
0
-5
-10
meadow
steppe
cushion
shrubland
forest
vegetation